Supporting Information

Large In-plane Piezo-strain Enhanced Voltage Control of Magnetic Anisotropy in Si-compatible Multiferroic Thin Films

*Bin Peng, Qi, Lu, Haowen Tang, Yao Zhang, Yuxin Cheng, Ruibin Qiu, Yunting Guo, Ziyao Zhou, and Ming Liu**

Electronic Materials Research Laboratory, Key Laboratory of the Ministry of Education & International Center for Dielectric Research, School of Electronics and Information Engineering, State Key Laboratory for Mechanical Behavior of Materials, International Joint Laboratory for Micro/Nano Manufacture and Measurement Technology, Xi'an Jiaotong University, Xi'an 710049, P. R. China
E-mail: mingliu@xjtu.edu.cn

Experimental

Deposition of multiferroic thin films: In the beginning, 4% Nb-doped $PbZr_{0.4}Ti_{0.6}O_3$ (PZT) thin films were fabricated by the chemical solution deposition method on platinized silicon substrates. The precursor solution was prepared by a modified 2-methoxyethanol synthesis route, using titanium isopropoxide, zirconium n-propoxide, lead acetate trihydrate, and niobium ethoxide as raw materials. Its concentration was 0.7 mol/L, and 20 mol% excess lead was added to the solution to compensate the lead loss during thermal annealing. We repeated spin-coating, pyrolysis, and annealing three times to obtain the desired thickness. The control samples are based on commercially available PZT-5H piezoelectric ceramics (t=1 mm, Baoding Hongsheng, Inc.) and PMN-PT single crystals (t=0.5 mm or 1 mm, Crystal Lab of Laser Technology Research Center, Anhui Institute of Optics and Fine Mechanics). Both PZT-5H ceramics and PMN-PT single crystals were polished by Anhui Institute of Optics and Fine Mechanics. The ferroelectric thin films, ceramics or single crystals were transferred to the chamber of magnetron sputtering (Phase II, AJA International) to deposit metallic thin films, such as Ta, Pt, Au, NiFe, and CoFeB, with a base pressure $<1\times10^{-7}$ Torr, a working Ar pressure of 3 mTorr and DC power of 20-30 W. The insulating layer, SiO_2, was deposited by RF sputtering with a power of 150 W. A quartz crystal microbalance monitored the thickness of the metallic films and SiO_2 within the sputtering system. The electrode size and patterns of micro-FMR devices were defined by photolithography and lift-off. For electrical measurement, the top Pt layer has a thickness of about 100 nm. For micro-FMR measurement, the recipes are Ta(1 nm)/NiFe(6 nm)/Pt(9 nm), and Ta(1 nm)/CoFeB(4 nm)/Pt(3 nm), along with SiO_2 (100 nm) and Au (100 nm).

Materials microstructure characterization: The crystalline structure was characterized using an X-ray diffraction system (PANalytical Empyrean). The film thickness was obtained from cross-sectional scanning electron microscopy (SEM) (FEI

Quanta FEG250). The surface morphology was characterized by atomic force microscopy (AFM) (Bruker Icon).

Electrical and magnetic measurements: The dielectric properties were measured by a precision LCR meter (Agilent E4980A). A ferroelectric analyzer (aixACCT TF2000) with a double beam laser interferometer (aixDBLI) was employed to evaluate the ferroelectric and piezoelectric properties of PZT thin films. The same ferroelectric analyzer was also used to characterize ferroelectric polarization and piezoelectric strain of ceramics and single crystals. The breakdown behavior of thin films was characterized by a source/measurement unit (Agilent B2901A), and voltage was applied automatically by the software. It was also used to apply DC voltage to ferroelectric thin films during micro-FMR measurement. The breakdown voltage of ceramics and single-crystals was characterized by a withstanding voltage tester (RK2674A), and voltage was applied manually by a knob. The bulk samples were immersed in silicone oil during the breakdown test. Conventional narrow-band FMR spectra were recorded using a high sensitivity X-band (~9.3 GHz) electron paramagnetic resonance system (JEOL JES-FA200). We use an electrometer (Keithley 6517B) to apply voltage to bulk samples, whose voltage limit is 1000 V. M-H hysteresis loops were measured on a vibrating sample magnetometer (Lake Shore 7404). Micro-FMR measurement was conducted on a customized spin-torque FMR system, including a lock-in amplifier (Stanford SR810), an RF/microwave signal generator (Keysight N5173B), a bias tee (Picosecond Pulse Lab 5530B), and a probe station.

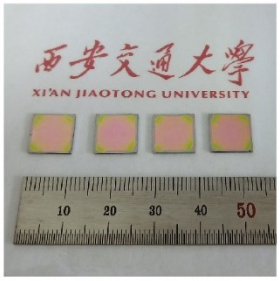

Figure S1 Optical images of PZT thin films. Those thin films were deposited on platinized silicon substrates by spin coating, and the substrates have a size of 1 cm × 1 cm.

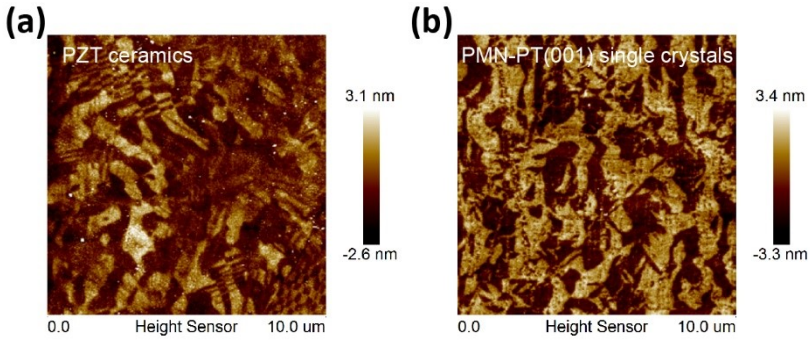

Figure S2 Surface AFM images of (a) PZT ceramics and (b) PMN-PT(001) single crystals. The average roughness for ceramics and single-crystals is 0.686 nm and 1.11 nm, respectively. They and PZT thin films are very smooth. The contrast in this figure

indicates the existence of relatively large ferroelectric domains in bulk samples.

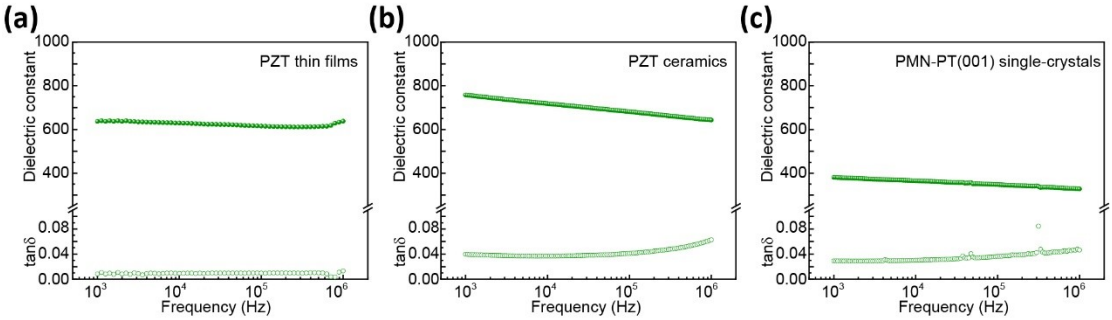

Figure S3 Frequency-dependent dielectric properties of (a) PZT thin films, (b) PZT ceramics, and (c) PMN-PT (001) single-crystals. All the samples have relatively stable frequency-dependent dielectric properties. The dielectric constant at 10 kHz are 630, 718, and 365, respectively. The dielectric loss are 1.1%, 3.7% and 3.0%, respectively. PZT thin films have the smallest dielectric loss, indicating thin films have fewer defects.

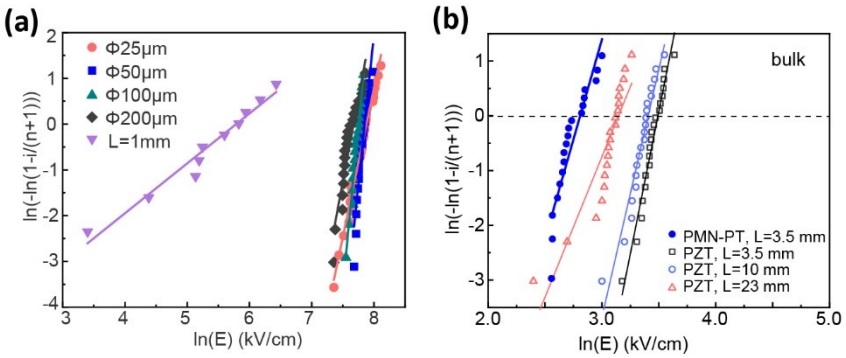

Figure S4 Weibull plot of breakdown field for (a) PZT thin films and (b) PZT ceramics and PMN-PT single crystals with varied electrode sizes. The breakdown electric fields of dielectrics usually follow a two-parameter Weibull distribution, and the average dielectric strength can be determined from the variation between different tests according to X_i=ln(E_i) and Y_i=ln(-ln(1-i/(n+1))), where X_i and Y_i are two parameters in the Weibull distribution function, E_i is the breakdown electric field in each test, n is the number of tests, and i is the serial number. The breakdown fields increase in the order of $E_1 \leq E_2 \leq \ldots \leq E_i \leq \ldots E_n$. Through the linear fitting of $Y_i(X_i)$ curves, the average dielectric strength E_b was obtained, and E_b is X_i at Y_i=0.

Table S1 Size-dependent breakdown strength for PZT thin films.

Electrode area (μm^2)	Electrode size	Average E_b (MV/cm)	Error (MV/cm)	Maximum E_b (MV/cm)
491	D=25μm	2.643	0.05	3.20
1963	D=50μm	2.568	0.24	2.93
7854	D=100μm	2.333	0.08	2.53
31414	D=200μm	2.147	0.23	2.60
1000000	L=1mm	0.326	0.01	0.62

Table S2 Size-dependent breakdown strength for PZT ceramics.

Electrode area (μm^2)	Electrode size	Average E_b (MV/cm)	Error (MV/cm)	Maximum E_b (MV/cm)
12250000	L=3.5mm	0.033	0.0013	0.038
100000000	L=10mm	0.030	0.0021	0.035
529000000	L=23mm	0.023	0.0045	0.026

Table S3 Size-dependent breakdown strength for PMN-PT single-crystals

Electrode area (μm^2)	Electrode size	Average E_b (MV/cm)	Error (MV/cm)	Maximum E_b (MV/cm)
12250000	L=3.5mm	0.017	0.0023	0.020

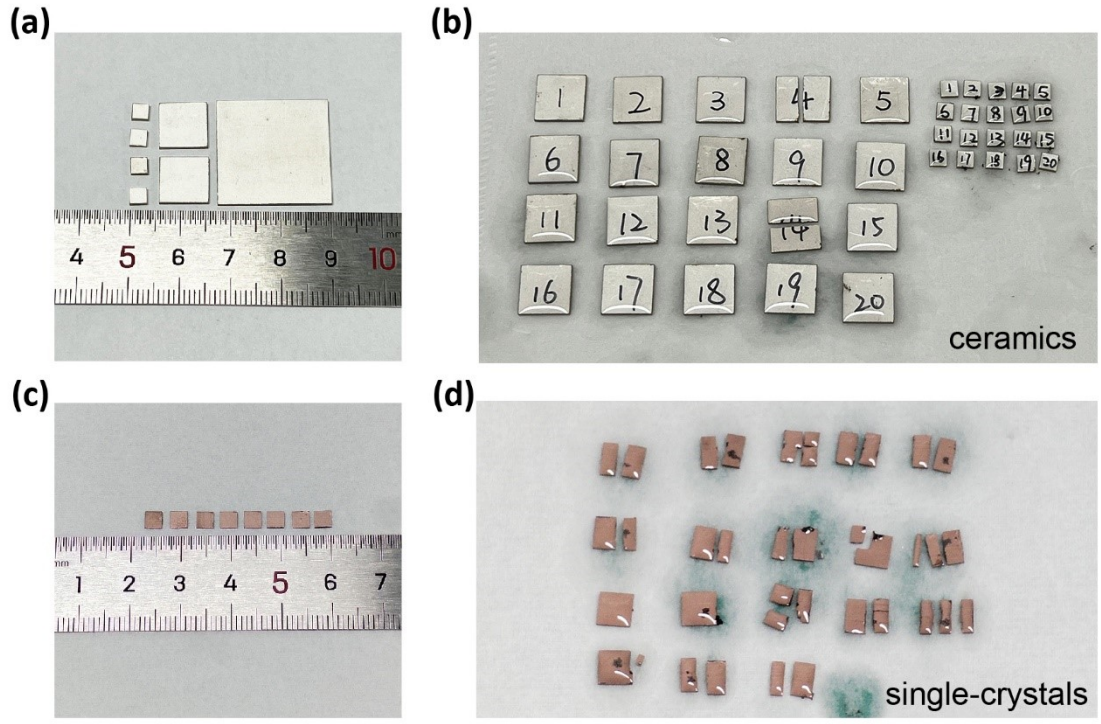

Figure S5 Optical images of PZT ceramics (a) before and (b) after breakdown, PMN-PT single crystals (c) before and (d) after breakdown. Most PZT ceramics remain intact, and only two samples crack after breakdown. Especially for the smallest ceramics (3.5 mm× 3.5 mm), no sample cracks. However, for PMN-PT single crystals, nearly all the samples crack after breakdown, indicating an electro-mechanical failure.

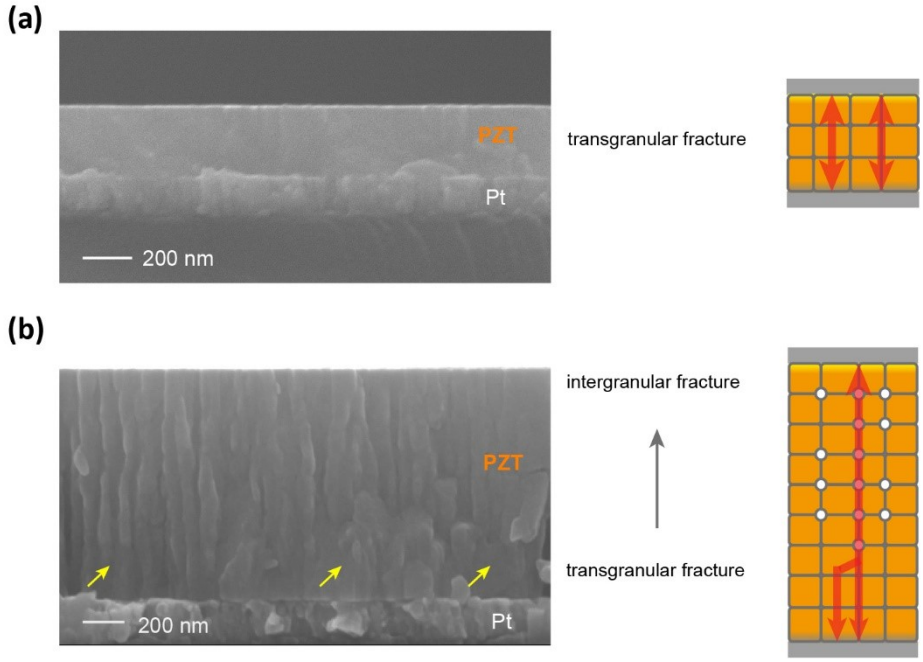

Figure S6 Cross-sectional SEM images of PZT (a) thin films and (b) thick films. Those films have distinct mechanical properties. The thin films exhibit transgranular fracture behavior, and the thick films exhibit intergranular fracture behavior. We could observe columnar grains of PZT thick films (~1 μm) and even the interface of different deposited layers in figure b. However, such grains and interfaces in thin films could not be observed from cross-sectional SEM, and their microstructure is relatively uniform. The difference in mechanical properties between grains and grain boundaries in thin films is negligible. Usually, it is the accumulated defects at grain boundaries that deteriorate the mechanical properties. Therefore, we expect the difference in electrical properties between grains and grain boundaries in thin films is also very small. However, for thick films, grain boundaries will be the easiest path for electrical conduction.

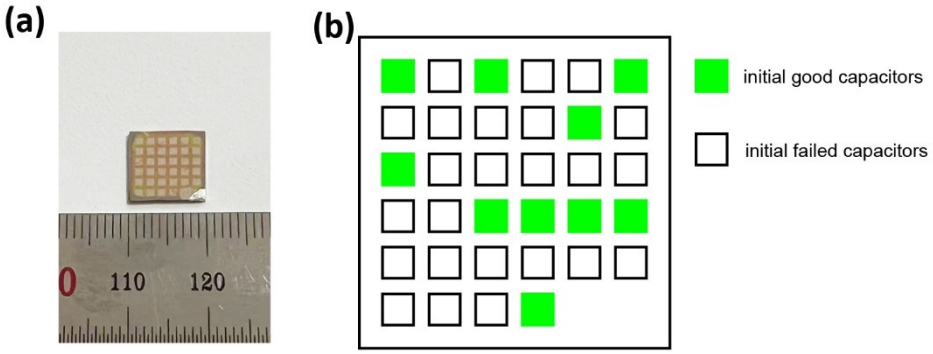

Figure S7 (a) Optical images of PZT thin films with large top electrodes after breakdown, (b) initial check of capacitors before breakdown test. The largest top electrode on PZT thin films has a size of 1 mm×1 mm, and it is prepared by photolithography. We checked those capacitors, and only 29% of them (10/34) are good

capacitors. Most of the capacitors failed the test. They became conducting at a low voltage (1 V) and behaved as resistors.

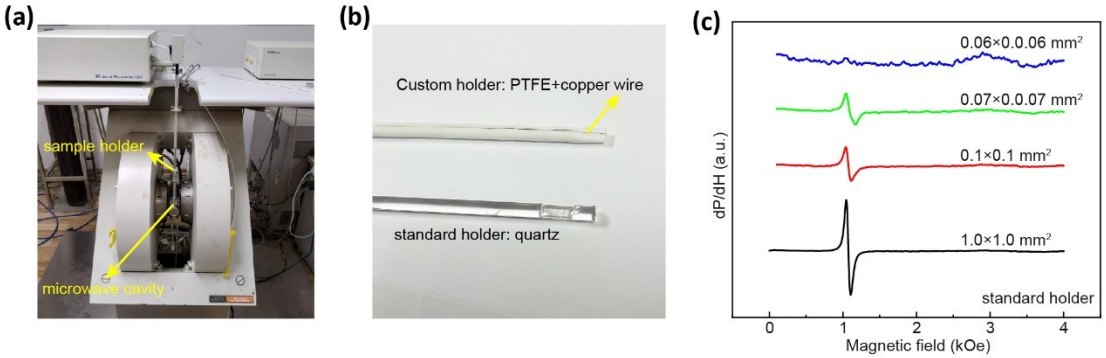

Figure S8 (a) optical images of the instrument for conventional VCMA test of bulk samples, (b) standard and custom sample holder, (c) FMR spectra for PZT thin films/NiFe (6 nm) with different top electrode sizes. Conventional VCMA test of bulk samples is usually conducted on a commercial electron paramagnetic resonance (EPR) spectrometer and in a microwave cavity. The standard sample holder is made of quartz. To apply voltage, we have designed a custom holder made by PTFE and use copper wires for electrical connection. Compared to quartz, PTFE and copper wires are lossy at the microwave frequency and will degrade the quality factor of the microwave cavity. Consequently, that will also degrade the sensitivity of EPR. Although we could test "PZT thin films/NiFe" samples with smaller top electrode sizes (Figure c) using a standard holder, it is difficult to apply voltage. In addition, we need a relatively large top electrode size for electrical connection.

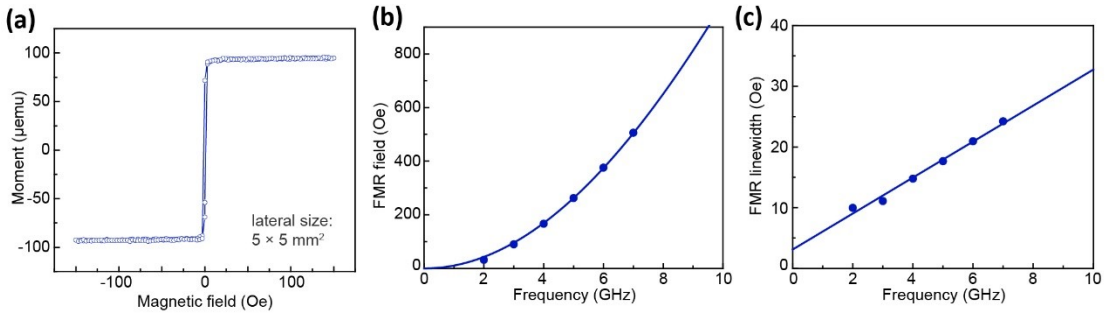

Figure S9 (a) Magnetization hysteresis loops of PZT/NiFe thin films with a lateral size of 5 mm×5 mm. **Measured and fitted microwave frequency-dependent (b) FMR fields and (c) FMR linewidth from micro-FMR measurement.** Based on Equation (1), the FMR fields and FMR linewidth were extracted from Figure 4c. Figure S9b shows both the measured and the fitted frequency-dependent FMR fields (H_r-f curves), from which the effective magnetization was estimated to be $4\pi M_{eff}$=11.8 kOe by Kittel equations. Figure S9c shows both the measured and the linearly fitted frequency-dependent FMR linewidth, corresponding to magnetic damping constant about 1.32×10^{-3}.

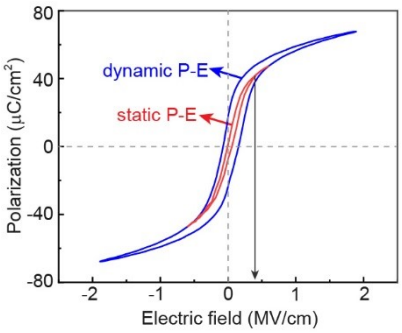

Figure S10 Dynamic and static *P-E* loops for PZT thin films. During *P-E* measurement, the recorded surface charge of capacitors mainly comes from ferroelectric polarization when the electric field is close to the coercive field. At high field, the surface charge mainly comes from the linear dielectric response. During our micro-FMR measurement, the voltage on the ferroelectric layer is applied in a static mode. The static *P-E* hysteresis loops have a lower coercive field as compared to the dynamic *P-E* loop. It reaches linear and hysteresis-free regions also at a relatively small electric field below 0.5 MV/cm.

Table S4 Summary of VCMA effect for “PMN-PT single crystal/CoFeB thin film” from literature.

Materials	VCMA	Experimental results	Ref
PMN-30PT(001) (0.5 mm)/$Co_{40}Fe_{40}B_{20}$(20 nm)	Strain from linear piezoelectric effect $\Delta H_{k,max}$=22 Oe for ΔE=6kV/cm Strain from other effect $\Delta H_{k,max}$=64 Oe for ΔE=6kV/cm	Strain from linear piezoelectric effect Type I Hk=11.0 mT @ +0kV/cm, Hk=8.2 mT @ +6kV/cm (Fig 2a) Hk=11.6 mT@-0 kV/cm, Hk=11.4 mT @ -6kV/cm (Fig 2a) Type II Hk=8.6 mT @ +0 kV/cm, Hk=8.4 mT @ +6 kV/cm (Fig 2b) Hk=9.0 mT @ -0 kV/cm, Hk=8.0 mT @-6 kV/cm (Fig 2b) Type III Hk=4.2 mT @ +0 kV/cm, Hk=2.2 mT @ +6 kV/cm (Fig 2c) Hk=8.6 mT @ -0 kV/cm, Hk=10.2 mT @-6 kV/cm (Fig 2c) Strain from ferroelastic domain switching Type III Hk=4.2 mT @ +0 kV/cm, Hk=10.2 mT @-6 kV/cm (Fig 2c) Hk=8.6 mT @ -0 kV/cm, Hk=2.2 mT @ +6 kV/cm (Fig 2c)	[1]
PMN-PT(011)/CoFeB(4 nm)	Strain from linear piezoelectric effect $\Delta H_{k,max}$=9 Oe forΔE= 8 kV/cm Strain from other effect $\Delta H_{k,max}$=22 Oe forΔE= 2.4 kV/cm	Strain from linear piezoelectric effect H//+135° Hr=35.9 mT@+0 kV/cm, Hr=35.4 mT@+8 kV/cm (Fig 1f) Hr=36.2 mT@-0 kV/cm, Hr=35.7 mT@-8 kV/cm (Fig 1f) H//+45° Hr=36.9 mT@+0 kV/cm, Hr=37.5 mT@+8 kV/cm (Fig 1f) Hr=36.1 mT@-0 kV/cm, Hr=37.0 mT@-8 kV/cm (Fig 1f) Strain from ferroelastic domain switching	[2]

		H//+45° ΔHr=2.2 mT 0→+2.4kV/cm (Fig 2a)	
PMN-18PT(001) (0.5 mm)/$Co_{40}Fe_{40}B_{20}$(20 nm)	Strain from other effect $\Delta H_{k,max}$=72 Oe for ΔE =8kV/cm	Strain from ferroelectric phase transition In-plane [100] direction Hr= 665 Oe @0 kV/cm (Fig 2c), Hr=737 Oe @+8 kV/cm (Fig 2f) In-pane [010] direction Hr=668 Oe @0 kV/cm (Fig 2c), Hr=703 Oe @+8 kV/cm (Fig 2f)	[3]
PMN-30PT(011) (0.5 mm)/$Co_{20}Fe_{60}B_{20}$(100 nm)	Strain from other effect $\Delta H_{k,max}$=193.8 Oe for ΔE=10 kV/cm	Strain from anisotropic in-plane piezoelectric effect Hr=696.7 Oe @+0 kV/cm, Hr=874.4Oe @+10 kV/cm (Fig 2b) Hr=720.8 Oe @-0 kV/cm, Hr=914.6 Oe @-10 kV/cm (Fig 2d)	[4]
PZT (290 nm)/ $Co_{40}Fe_{40}B_{20}$ (4 nm)	Strain from linear piezoelectric effect $\Delta H_{k,max}$=26.1 Oe for ΔE=1.03 MV/cm		Our work

References

1. Y. Ba, Y. Liu, P. Li, L. Wu, J. Unguris, D. T. Pierce, D. Yang, C. Feng, Y. Zhang, H. Wu, D. Li, Y. Chang, J. Zhang, X. Han, J. Cai, C.-W. Nan and Y. Zhao, *Adv. Funct. Mater.*, 2018, **28**, 1706448.
2. T. Nan, J.-M. Hu, M. Dai, S. Emori, X. Wang, Z. Hu, A. Matyushov, L.-Q. Chen and N. Sun, *Adv. Funct. Mater.*, 2019, **29**, 1806371.
3. C. Feng, Y. Liu, H. Huang, Z. Zhu, Y. Yang, Y. Ba, S. Yan, J. Cai, Y. Lu, J. Zhang, S. Zhang and Y. Zhao, *ACS Appl. Mater. Interfaces*, 2019, **11**, 25569-25577.
4. A.-p. Wang, M. Feng, C.-l. Qi, M. Liv, H.-s. Jia, W. Wang, Y.-l. E, L.-l. Hu, W. Wang and H.-b. Li, *Scripta Mater.*, 2020, **179**, 80-85.